arXiv:astro-ph/0005312 15 May 2000

Evolution in the Clustering of Galaxies for $z < 1.0$

Robert J. Brunner[1]

Department of Astronomy, The California Institute of Technology, Pasadena, CA 91125

rb@astro.caltech.edu

Alex S. Szalay[1]

Department of Physics and Astronomy, The Johns Hopkins University, Baltimore, MD 21218

szalay@pha.jhu.edu

Andrew J. Connolly[1]

Department of Physics and Astronomy, University of Pittsburgh, Pittsburgh, PA, 15260

ajc@phyast.pitt.edu

ABSTRACT

Measuring the evolution in the clustering of galaxies over a large redshift range is a challenging problem. We have developed a new technique which uses photometric redshifts to measure the angular correlation function in redshift shells. This novel approach minimizes the galaxy projection effect inherent in standard angular correlation measurements, and allows for a measurement of the evolution in the galaxy correlation strength with redshift. In this paper, we present new results which utilize more accurate photometric redshifts, which are derived from a multi-band dataset (U,B,R, and I) covering almost two hundred square arcminutes to $B_{AB} \sim 26.5^m$, to quantify the evolution in the clustering of galaxies for $z < 1$. We also extend our technique to incorporate absolute magnitudes, which provides a simultaneous measurement of the evolution of clustering with both redshift and intrinsic luminosity. Specifically, we find a gradual decline in the strength of clustering with redshift out to $z \sim 1$, as predicted by semi-analytic models of structure formation. Furthermore, we find that $r_0(z = 0) \approx 4.0h^{-1}$ Mpc for the predictions of linear theory in an $\Omega_0 = 0.1$ universe.

Subject headings: cosmology: observations— galaxies: evolution—galaxies: photometry

---

[1]Visiting Astronomer, Kitt Peak National Observatory, National Optical Astronomy Observatories, which is operated by the Association of Universities for Research in Astronomy, Inc. (AURA) under cooperative agreement with the National Science Foundation.

1. Introduction

One of the key problems in modern astronomy is understanding how galaxies form and evolve. Although this problem might seem rather straightforward, a considerable amount of uncertainty remains, primarily because of the difficulty in separating out the competing effects of density evolution, *i.e.* variation in the number of galaxies with redshift due to clustering or mergers, from luminosity evolution, *i.e.* the intrinsic evolution in an individual galaxy's spectral energy distribution.

Historically, two principle techniques have been used to quantify evolution in the clustering of galaxies. The first technique is to invert the angular correlation function ($w(\theta)$) using the Limber equation (Limber 1954; Peebles 1980) and an observed or model redshift distribution to estimate the expected change in the amplitude of the angular correlation function for different magnitude intervals and/or cosmologies(*e.g.*, Koo & Szalay 1984; Efstathiou *et al.* 1991; Roche *et al.* 1993; Infante & Pritchet 1995; Brainerd *et al.* 1996). The alternative approach is to compute the spatial correlation function ($\xi(r)$) for different epochs directly using spectroscopic redshifts (Le Fèvre *et al.* 1996; Carlberg *et al.* 1997, 1999; Small *et al.* 1999). These two techniques, however, suffer from different limitations that have restricted their utility.

Studies which utilize different magnitude intervals are limited in that an apparent magnitude selection samples galaxies of different intrinsic luminosities at different redshifts, complicating the analysis considerably. Furthermore, the clustering of galaxies on small scales is the result of a highly non-linear, complex process; and, therefore, the actual validity of the power law model for the evolution of the spatial clustering function is not guaranteed, although it is at least a useful diagnostic. Finally, this approach is also limited by the applicability of the assumed redshift distribution, which can heavily influence the theoretical conversion from angular coordinates to spatial coordinates.

The spectroscopic approach, on the other hand, is hindered either by the size of the available samples, especially when the data is binned into distinct redshift intervals, or by the depth or width of the survey (which implies either a redshift variable, intrinsic luminosity selection effect or possible contamination from strong clustering). For example, Le Fèvre *et al.* (1996) analyze the spatial clustering for 591 galaxies in the CFRS with $I < 22.5$, Small *et al.* (1999) analyze the spatial clustering of 831 galaxies with $r \leq 21^m$ to measure the evolution in the correlation length for $0.2 \leq z \leq 0.5$, and Carlberg *et al.* (1997) use a sample of 248 galaxies with $K < 21.5$ while Carlberg *et al.* (1999) use 2300 high intrinsic luminosity galaxies distributed over a wide area, to determine the spatial correlation function for different epochs.

In this paper, we continue our development of a new technique which uses photometric redshifts to measure the angular correlation function in redshift shells (Brunner 1997; Connolly *et al.* 1998; Brunner *et al.* 1999b). This novel approach minimizes the galaxy projection effect inherent in standard angular correlation measurements, while utilizing a significantly large sample that minimizes the effects of shot noise in our analysis. By adopting an ensemble approach, we are able to measure the evolution of clustering with both redshift and intrinsic luminosity. Unless otherwise noted, we assume $h = 1.0$, $\Omega_M = 0.3$, and $\Omega_\Lambda = 0.7$, throughout this paper.

2. Data

The observations and reduction of the data used in this analysis have been extensively detailed elsewhere (Brunner 1997; Brunner *et al.* 1997, 1999a). In this section, we discuss the important points which impact the rest of our discussion.

2.1. Observations

The photometric data analyzed in this paper are located at 14:20, +52:30 covering approximately 0.054 square degrees. All of the photometric data were obtained using the Prime Focus CCD (PFCCD) camera on the Mayall 4 meter telescope at Kitt Peak National Observatory (KPNO). The observations were performed on the nights of March 31 – April 3, 1995, March 18 – 20, 1996, and May 14 – 16, 1996. The PFCCD uses the T2KB CCD, a 2048^2 Tektronix CCD with 24μm pixel scale, which at $f/2.8$ in the 4 meter results in a scale of $0.47''$/pixel and a field of view of $\approx 16.0' \times 16.0'$. All observations were made through the broadband filters: $U, B, R, \& \ I$.

2.2. Data Reduction

The photometric data were reduced in the standard fashion. The data were photometrically calibrated to the published Landolt (1992) standard star fields using a curve of growth analysis. A linear regression on the published stellar magnitude, the instrumental magnitude, the airmass, and a color term was performed, and the result translated to a one second standard exposure. We transformed our magnitude system to the AB system (Oke & Gunn 1983) using published transformations (Fukugita *et al.* 1995).

Source detection and photometry were performed using SExtractor version 2.0.8 (Bertin & Arnouts 1996) with the appropriate correction for the background estimation bug applied (Bertin 1998). SExtractor was chosen for its ability to perform matched aperture photometry, using the same detection image for each program image. Our detection image was constructed from the $U, B, R, \& \ I$ images using an optimal χ^2 process (Szalay *et al.* 1998).

The astrometric solution for our data was determined by matching against a pre-release version of the *HST* Guide Star Catalog II (Lasker 1996). The residuals of the final geometric transformation to the GSCII for the reference stars were all less than 0.15 pixels, or equivalently, less than $0.07''$.

Our completeness limits were calculated by adding artificially generated galaxies to the final stacked image. The iterative, Monte-Carlo approach we used produced a completeness curve, from which both a 90% and 50% completeness limits in all four bands were extracted. The 2% and 10% photometric error magnitude limits were calculated as the mean of all valid detections in the master catalog which had a measured photometric error that was approximately the same as the target photometric error (0.1 magnitudes for 10% photometry and 0.02 magnitudes for 2% photometry).

We empirically determined the stellar locus in each band separately using several complementary techniques: the ratio of a core to total magnitude, objects which were classified as stars on overlapping *HST* images, and objects which were spectroscopically identified as stars. In addition, all objects with $I < 20^m$ were visually inspected and classified as stellar or non-stellar. The final classification was constructed by taking the union of the four separate classifications in each band, resulting in 505 stellar objects. The number-magnitude distribution of stellar objects agrees with model predictions (Bahcall and Soneira 1980). The spatial distribution of the stellar objects is fairly random, with the possible minor exception of the image corners where the PSF increases due to focal degradations. As a result, these areas were not utilized during the actual correlation analysis.

2.3. Photometric Redshifts

Many cosmological tests are more sensitive to the sample size (*i.e.* Poisson Noise) than small errors in distance, which makes them perfect candidates for utilizing a photometric redshift catalog, including quantifying the evolution of galaxy clustering. As a result, we have developed an empirical photometric redshift technique (Connolly *et al.* 1995; Brunner *et al.* 1997; Brunner 1997; Brunner *et al.* 1999a), which is not designed to accurately predict the redshift for a given galaxy (Baum 1962) or locate high redshift objects (Steidel *et al.* 1996). Instead, it is designed to provide distance indicators which are statistically accurate for the entire sample, along with corresponding redshift error estimates.

The calibration data for implementing this technique was taken from overlapping spectroscopic surveys including data from both the Canada France Redshift survey (Lilly *et al.* 1995), and the Deep Extragalactic Evolutionary Probe survey (Mould 1993). The accuracy of any empirically derived relationship is predominantly dependent on the quality of the data used in the analysis — photometric redshifts being no exception. As a result, we imposed several restrictions on the calibrating data in order to minimize the intrinsic dispersion within the photometric redshift relationship. After imposing our quality assurance conditions, we were left with 190 galaxies which formed our calibration sample.

The 190 calibrating redshifts were, therefore, used to derive an iterative piecewise polynomial fit to the galaxy distribution in the $U, B, R, \&\ I$ flux space. This iterative approach utilizes a global fit to determine a rough estimate of the galaxy's redshift, after which a more accurate local polynomial fit, corresponding to the appropriate redshift interval, was applied (Brunner *et al.*

1999a). For each derived polynomial fit, the degrees of freedom remained a substantial fraction of the original data (a second order fit in four variables requires 15 parameters while a third order fit in four variables requires 35 parameters).

To estimate the error in a photometric redshift for the full photometric sample, we adopt a bootstrap with replacement algorithm, in which galaxies are randomly selected from the calibration sample and, once selected, are not removed from the set of calibrating galaxies. Thus, at the extremes, one galaxy could be selected 190 consecutive times or, alternatively, each redshift could be selected exactly once (each of these realizations has the same probability). This approach is designed to emphasize any incompleteness in the sampling of the true distribution of galaxies in the four dimensional space $U, B, R,$ & I by the calibration redshifts. In order to fully account for potential sources of error in the redshift estimation, the magnitudes of the calibrating sample were drawn from a Gaussian probability distribution function with mean given by the measured magnitude and sigma by the magnitude error.

The actual photometric redshift error was calculated from 100 different realizations using this algorithm. For each different realization, a photometric redshift was calculated for every galaxy in the photometric redshift catalog. The actual error was optimally determined to be given by the normalized difference between the fifth and second quantiles of the estimated redshift distribution for each individual galaxy (Brunner *et al.* 1999a). As expected the average estimated error is the largest at the upper and lower redshift limits where the incompleteness in the calibrating sample is most evident. The majority of the rest of the objects with extremely large redshift errors are blended in one or more bands, which causes these objects to be isolated from the high density surface delineated by the majority of galaxies in the four flux space $U, B, R,$ & I. The effect these objects impart on any subsequent analysis, however, is minimized by the inclusion of their photometric error, which causes them to be non-localized in redshift space. As a result, these objects provide a minimal contribution to many "redshift bins" rather than strongly biasing only a few bins.

A subtle, and often overlooked, effect in any photometric redshift analysis is the requirement for reliable photometry in all program filters. Ideally we would obtain accurate redshift estimates for all galaxies; however, since we need accurate, multi-band photometry in order to reliably estimate redshifts, we must place restrictions on the photometric catalog used in the analysis. In particular, we restrict the full sample of detected sources to those objects which have both $I_{AB} < 24.0$ and measured magnitude errors < 0.25 in $U, B,$ & R. This minimizes any selection bias to only faint early-type galaxies at high redshifts, or very high redshift drop-out objects (see Brunner *et al.* 1999a for more discussion), neither of which significantly affect the rest of our analysis.

3. Ensemble Approach

Due to the lower precision of photometric redshift determination as compared to spectroscopic redshifts (roughly a factor of 20), we have developed a new, statistical approach to quantifying the evolution of galaxies (Brunner 1997; Connolly *et al.* 1998; Brunner *et al.* 1999a). This approach capitalizes on our ability to reliably generate not only a redshift estimate for a galaxy using broadband photometry, but also a reliable redshift error estimate. As a result, we define the probability density function, $P(z)$, for an individual galaxy's redshift to be a Gaussian probability distribution function with mean (μ) given by the estimated photometric redshift and standard deviation (σ) defined by the estimated error in the photometric redshift.

$$P(z) = \frac{1}{\sigma\sqrt{2\pi}} e^{\left(-\frac{(z-\mu)^2}{2\sigma^2}\right)}$$

In order to measure an interesting cosmological quantity, we generate multiple ensembles (or realizations) of the relevant properties of the galaxy distribution using the statistical redshift and redshift error estimates (see Brunner *et al.* 1999a for an application of this technique to the number-redshift distribution). The quantity of interest is determined as the mean of the multiple realizations, and the associated error is given by the corresponding standard deviation.

In order to divide our sample by intrinsic luminosity, we determined the absolute magnitude distribution of the galaxies in our catalog in an ensemble approach. First, we created different realizations of our galaxy catalog. In order to minimize any systematic errors, we selected the apparent magnitude of each galaxy from a Gaussian probability distribution function with mean and sigma given from the original photometric catalog measurements. Similarly, the redshift of each galaxy was drawn from a separate Gaussian probability distribution function with mean and sigma given from the photometric redshift and corresponding redshift error estimate. The $k-$correction was determined using the spectral classification which was part of the original redshift estimation procedure. For galaxies with large photometric redshifts, occasional discordant redshifts were calculated (*i.e.* outside the range of our calibration sample — $z < 0$, or $z > 1.2$) in which case the galaxy was dropped from that particular realization.

Together, these quantities were used to determine the absolute magnitude for each galaxy in 100 different ensemble distributions. The absolute magnitude for each galaxy was calculated as the mean over the different realizations, appropriately normalized to account for possible discordant redshifts as discussed above. The resultant distributions for the U and B bands are displayed in Figure 2.

4. Analysis

Before computing the angular correlation function, we quantified our efficiency in detecting galaxies as a function of pixel location. The primary areas where this effect is important are around bright stars, in charge transfer trails, and near the edge of the frame due to edge effects or focus degradations. We, therefore, defined bounding boxes, for each of the four stacked images, which contained all of the observable flux for the saturated stars within the image. In the end, a total of 15 regions were masked out in the U frame, 17 regions were masked out in the B frame, 45 regions were masked out in the R frame, and 36 regions were masked out in the I frame. We also masked both the edge and corners of each frame in order to reduce the effects of PSF variations on our object detection efficiency. These four mask files were concatenated to produce a total mask file which was used for the calculation of the angular correlation function in different redshift or absolute magnitude intervals.

We used the optimal estimator Landy & Szalay (1993) $(DD-2DR+RR)/RR$, where D stands for data and R stands for random, to determine the angular correlation function. This required counting the number of observed pairs (that were not within masked areas), which was done in 10 bins of constant width $\Delta \lg(\theta) = 0.25$, centered at $\theta = 4.3''$, to $\theta = 759.6''$. One thousand objects were randomly placed in the non masked areas within the image, and the data-random (DR) and random-random (RR) correlation functions were calculated for the same angular bins used for the data-data (DD) auto-correlation function. Before applying the estimator, each of the correlation measurements were scaled by the appropriate number of pairs. This process was repeated ten separate times, and the results averaged to minimize any systematic effects.

This estimator uses the calculated number density of galaxies within the CCD frame to estimate the true mean density of galaxies. The small angular area of our images introduces a bias in the estimate, commonly referred to as the "Integral Constraint" (Peebles 1980). We estimated a correction for this bias following the prescription of Landy & Szalay (1993), which is subtracted from the estimated value.

The error in the estimation of the angular correlation function was assumed to be Poisson in nature. As a result, we calculated the error in the angular correlation estimation as the square root of the number of random-random pairs in each angular bin, scaled by the relevant number of data points.

The angular correlation function is generally parameterized in the following fashion:

$$w(\theta) = A_w \theta^{-\delta}$$

where the exponent has previously been shown to be $\delta = 0.8$. In general, the amplitude of the correlation function (A_w) is calculated (assuming the previous value for δ) by minimizing the χ^2 with respect to A_w (Press *et al.* 1992):

$$A_w = \left(\sum_{i=1}^{N} \lg(w(\theta)_i) + 0.8 \sum_{i=1}^{N} \lg(\theta_i) \right) /N$$

This calculation can be significantly affected by outliers; and, as a result, we adopt the more robust technique of minimization of the absolute deviations to determine the angular correlation amplitude. For our simple case, this technique reduces to finding the median of the amplitudes at each angle (Press *et al.* 1992).

4.1. The Angular Correlation Function: $w(\theta)$

Although not the primary aim of this paper, we measured the angular correlation function in different apparent magnitude intervals to compare with previous work. For each program filter, the absolute upper magnitude limit for the data used in the estimation of the angular correlation function was set at the 90% catalog completeness limit and the lower magnitude limit was always set to 15^m. The angular correlation function was then determined in four different magnitude ranges (each offset from the next by 0.5^m). The upper magnitude limits, and the corresponding number of objects are listed in Table 1. Each estimation was repeated 100 times.

The amplitude of the different correlation functions for each band at $\theta = 1.0''$ are listed in Table 2. For brevity, we only display the results for the B band. Thus, in Figure 3 the actual correlation measurements for the different magnitude bins are displayed, while in Figure 4 the measured correlation amplitudes are compared to comparable published results (*e.g.*, Koo & Szalay 1984; Roche *et al.* 1993; Infante & Pritchet 1995), showing remarkably good agreement. The error bars were calculated from the one sigma upper and lower measurements of the amplitude of the angular correlation function.

4.2. The Multi-Variate Angular Correlation Function: $w(\theta, z)$

Using the 3052 objects in the photometric redshift–template SED catalog, the multivariate angular correlation function $w(\theta, z_P)$ was determined for four different redshifts by binning the data in non-overlapping redshift bins of width $\Delta z_P = 0.2$ centered at $z_P = 0.4$ to $z_P = 1.0$. The four different functions were calculated for the 445, 573, 946, and 582 objects in the different respective redshift bins. We display, in Figure 5, the measured change in the amplitude of the angular correlation function with redshift (*i.e.* A_w), and hence the strength of the angular correlation function at a fixed angular separation. The error in $A_w(z)$ was calculated by estimating the amplitude in each redshift interval for the one sigma upper and lower values.

In order to compare this result with theoretical expectations (*e.g.*, semi-analytic theory), which are determined in spatial coordinates, it is necessary to convert between angular correlation measurements and spatial correlation quantities. The standard technique for determining this transformation is to assume a power law model for the spatial clustering (Peebles 1980; Le Fèvre *et al.* 1996),

$$\xi(r, z) = \left(\frac{r}{r_0(z)}\right)^{-\gamma} = \left(\frac{r}{r_0(0)}\right)^{-\gamma} (1 + z)^{-(3+\epsilon)}$$

where ϵ represents a parameterization of the evolution of the spatial correlation function, and the correlation length is measured in physical units. The conversion, for small angular separations, between angular and spatial coordinates is accomplished via the relativistic form of Limber's equation (Limber 1954; Peebles 1980). Specifically, this results in the following conversion for the amplitude of the angular correlation function within the redshift region of interest:

$$A_w = \left(\frac{\int_0^\infty G(z) B(\gamma) (\frac{dN}{dz})^2 dz}{\left[\int_0^\infty \frac{dN}{dz} dz\right]^2} \right) r_0^\gamma \tag{1}$$

where,

$$G(z) = (1+z)^{-(3+\epsilon)} \sqrt{1 + \Omega_0\ z}\ x(z)^{(1-\gamma)},$$

$$B(\gamma) = \left(\frac{3600.0 * 180.0}{\pi} \right)^{(\gamma-1)} \left(\frac{H_0}{c} \right)^\gamma \frac{\Gamma(\frac{1}{2})\Gamma(\frac{(\gamma-1)}{2})}{\Gamma(\frac{\gamma}{2})}$$

is a constant quantity,

$$x(z) = 2 \frac{((\Omega_0 - 2)(\sqrt{1 + \Omega_0 z} + 2 - \Omega_0 + \Omega_0 z)}{\Omega_0^2 (1+z)^2},$$

is the angular diameter distance (Weinberg 1972), and dN/dz is the number of galaxies per unit redshift. Local spectroscopic surveys have determined that $\gamma \approx 1.8$ and $r_0 \sim 5.0$ Mpc in co-moving coordinates (Carlberg *et al.* 1999).

By assuming a uniform redshift distribution, we have calculated the tracks of different evolutionary models for $\Omega_0 = 1.0$ and $\Omega_0 = 0.1$, which are displayed, along with the measured values of the amplitude of the angular correlation function in Figure 5. Of the three different scenarios, fixed clustering in co-moving coordinates ($\epsilon = -1.2$) are the least consistent with our data, independent of the value of Ω_0. The results for clustering fixed in proper coordinates ($\epsilon = 0.0$) are good, independent of the value of Ω_0, while the predictions of linear theory ($\epsilon = 0.8$) are in agreement for higher values of Ω_0.

While this result is interesting, we can take an additional step in order to directly compare our measurements with published results from spectroscopic surveys. Using Equation 1 and an ensemble averaged empirical redshift distribution, we can actually transform our measurement of the angular correlation amplitude into a determination of the spatial correlation scale length within a given redshift interval, since we are able to empirically compute our observed redshift distribution (see Brunner *et al.* 1999a for more details). Essentially, this only involves adding a top-hat window function (corresponding to the appropriate redshift interval) to the integrands in Equation 1, since the transformation will be applied individually to each redshift bin in which we calculated the angular correlation amplitude.

The process is complicated, however, by the fact that our dN/dz is determined using photometric redshifts, while the transformation assumes a spectroscopic redshift interval. From Figure 1, although small, the dispersion between spectroscopic redshifts and photometric redshifts is not zero. The conversion between a spectroscopic interval and a photometric redshift interval accounts to a broadening of the top-hat function, which we accomplish using two Gaussians centered on the endpoints of the redshift interval, so that the new window function is given by

$$W(z) = \begin{cases} e^{\frac{-(z-z_1)^2}{\sigma^2}} & 0 \leq z < z_1 \\ 1 & z_1 \leq z \leq z_2 \\ e^{\frac{-(z-z_2)^2}{\sigma^2}} & z_1 < z < \infty \end{cases} ,$$

where the desired redshift interval is given by $z \in [z_1, z_2]$, and $\sigma = 0.061$ is the measured dispersion in the photometric redshift relation.

The results of the transformation determine the correlation length within the given redshift bin (*i.e.* $r_0(z)$), and are displayed in Figure 6 and also tabulated in Table 3 for $\Omega_0 = 0.1$, and the three canonical values of ϵ. In addition, the values of the correlation length extrapolated to $z = 0$ (*i.e.* $r_0(0)$) are tabulated in Table 4 for three different values of Ω_0. The strong dependence of the correlation scale length on the value of the evolutionary parameter (ϵ) is a direct result of the Cosmological term ($G(z)$) in Equation 1. Relative to the predictions of linear theory ($\epsilon = 0.8$), the results for fixed clustering in co-moving coordinates ($\epsilon = -1.2$), are suppressed by an additional factor of $\sim (1 + z)$, or roughly a factor of 1.5–2 at the redshifts of interest (recall that $r_0(z) \propto G(z)^{-\gamma}$).

When comparing our results to previous spectroscopic results, we clearly show excellent agreement with recent measurements (Carlberg *et al.* 1999; Small *et al.* 1999) when the predictions of linear theory are used to quantify the evolution of clustering. This is extremely encouraging for our technique, as we uniformly sample a larger redshift range, showing, for the first time within the same dataset, the slight decrease in the correlation strength for $z < 1$, as predicted by semi-analytic models of galaxy formation (Baugh et al. 1999). On the other hand, the measurement of the correlation scale length from the CFRS data (Le Fèvre *et al.* 1996) are only in agreement with our results for fixed clustering in co-moving coordinates, which disagrees with the hierarchical growth of dark matter halos (Baugh et al. 1999). The discrepancy between the CFRS and other measurements is most likely due to their relatively small sample size, their small fields, and their neglect of the redshift evolution of the Luminosity function (Carlberg *et al.* 1999).

4.3. The Multi-Variate Angular Correlation Function: $w(\theta, z, M)$

While important, the evolution of the angular correlation function with redshift smoothes over the galaxy luminosity function, ignoring variations in clustering between galaxies of different intrinsic luminosity. As a result, we subdivided our sample into three redshift intervals ($0.2 \leq z \leq 0.6$, $0.4 \leq z \leq 0.8$, $0.6 \leq z \leq 1.0$), and measured the angular correlation function as a function of both U and B absolute magnitude in intervals of 2.0^m, from 22^m to 12^m. In order to improve the number of galaxies in the faint end of our analysis, we rebinned the data so that the faint bin was four magnitudes wide (*i.e.* 16^m–12^m). In the end, we obtained twelve different measurements of the multivariate angular correlation function ($w(\theta, z, M)$) as a function of both U and B absolute magnitudes.

The number of subdivisions used in this particular analysis reintroduced one of the problems our new technique was designed to avoid, namely the effects of small sample size. We, therefore, only used a joint redshift-absolute magnitude bin when the number of objects in the bin exceeded one hundred galaxies. From Figures 7, 8 (U and B respectively), it is clear that there is no obvious evolution within a given redshift interval with intrinsic luminosity (although this could be a result of too few galaxies). Between redshift intervals, however, there is strong evolution in the amplitude of the angular correlation function (A_w), which, given the wider redshift bins, is completely consistent with the results of the previous section.

In order to quantify this evolution, we fit a line of zero slope to the points (*i.e.* a mean value for each redshift interval). Between the first two redshift bins (roughly $z \approx 0.4$ and $z \approx 0.6$), A_w drops by approximately a factor of two. For the U band measurement, the drop between the second and third redshift intervals (roughly $z \approx 0.6$ and $z \approx 0.8$) is approximately 20%, while the B band shows another factor of approximately two decline. This result is not surprising in the context of hierarchical structure formation where one expects objects to be more strongly cluster with decreasing redshift for $z < 1$ (*e.g.*, Kauffmann *et al.* 1999).

Unfortunately, we do not have enough galaxies to definitely test for clustering evolution with redshift for a given population with a fixed intrinsic luminosity. On the other hand, our results do seem to indicate that the evolution is not strongly dependent on intrinsic luminosity as there appears to be no clear evidence for variation in the clustering amplitude within a given redshift interval. The difference in the drop in the amplitude between the middle and high redshift intervals is most likely due to the lower, average intrinsic luminosity of the galaxies in the B band as compared to the U band. These points will need to be addressed with future datasets.

5. Conclusions

In this paper, we have presented several calculations of the angular correlation function, as a function of different apparent magnitude intervals, as a function of redshift, and as a function of both redshift and absolute magnitude. The technique we have demonstrated is less sensitive to redshift distortions than the spatial correlation approach due to the width of our redshift bins. Furthermore, our technique does not require model predictions for the redshift distribution of galaxies as does the apparent magnitude interval approach. Future work in this area will incorporate spectroscopic redshifts into the calculation in order to provide limited distance information (*cf.* Phillipps 1985), as well as witness the application of these techniques to larger surveys.

While not the main point of this paper, the variation of the amplitude of the angular correlation with apparent magnitude is in good agreement with previously published results, which strengthens the rest of our analysis. Furthermore, we demonstrated, for the first time from within a single dataset, the slight evolution in both the amplitude of the angular correlation function, and the spatial correlation scale length with redshift for $z < 1$, as predicted by semi-analytic models of structure formation (Baugh et al. 1999; Kauffmann *et al.* 1999). These results suggest low values for Ω_0, and allow either fixed clustering in proper coordinates, or the predictions of linear theory.

Finally, we measured the evolution of the amplitude of the angular correlation function with both redshift and intrinsic luminosity. The amplitude of the angular correlation function drops dramatically with redshift. Interestingly enough, however, we do not see significant variation in the strength of clustering within a given redshift interval as a function of intrinsic luminosity. This type of evolution might be naively expected if the luminosity of a galaxy uniquely mapped to the mass of the dark matter halo at the given redshift in which it resides (*i.e.* more luminous galaxies cluster more strongly within a given redshift interval). Most likely, either we have too small of a sample to place significant limits on the variation of clustering with luminosity, or else the relatively constant clustering amplitude as a function of luminosity is indicative of luminosity evolution complicating the analysis.

Future surveys, both photometric and spectroscopic (*e.g.*, SDSS) will provide extremely useful datasets with which we can explore these ideas in greater detail. In the near future, this area will witness a merging of observations, semi-analytic theory, and N-body simulations, finally providing hope that we will be able to unambiguously quantify the clustering evolution of galaxies.

First we wish to acknowledge Gyula Szokoly for assistance in obtaining the data. We also would like to thank Barry Lasker, Gretchen Greene, and Brian McLean for allowing us access to an early version of the GSC II. We also wish to acknowledge useful discussions with Pat Cote, Rich Kron, Lori Lubin, and Ray Weymann. We thank the anonymous referee for valuable suggestions on improving this work. This research has made use of NASA's Astrophysical Data System Abstract Service. AS acknowledges support from NASA LTSA (NAG53503) and *HST* Grant (GO-07817-04-96A), AJC acknowledges partial support from *HST* (GO-07817-02-96A) and LTSA (NRA-98-03-LTSA-039).

REFERENCES

Bahcall, J.N., & Soneira, R.M. 1980, ApJS, 44, 73.

Baugh, C. M., Benson, A. J., Cole, S., Frenk, C. S. & Lacey, C. G. 1999, MNRAS, 305, L21.

Baum, W.A. 1962, Problems of Extragalactic Research, IAU Symposium No. 15., 390.

Bertin, E., & Arnout, S. 1996, A&AS, 117, 393.

Bertin, E. 1998, Private Communication.

Brainerd, T.G., Blandford, R.D. & Smail, I. 1996, ApJ, 466, 623.

Brunner, R.J, 1997, PhD. Thesis, The Johns Hopkins University.

Brunner, R.J, Connolly, A.J., Szalay, A.S., & Bershady, M.A. 1997, ApJ, 482, L21.

Brunner, R.J, Connolly, A.J., & Szalay, A.S. 1999, ApJ, 516, 563.

Brunner, R.J, Connolly, A.J., & Szalay, A.S. 1999, In R. Weymann, L. Storrie-Lombardi, M.Sawicki, & R. Brunner, editors, *Photometric Redshifts and High-Redshift Galaxies*, number 191 in ASP Conference Series.

Carlberg, R.G., Cowie, L.L., Songalia, A., Hu & E.M. 1997, ApJ, 484, 538.

Carlberg, R.G., Yee, H.K.C., Morris, S.L., Lin, H., Hall, P.B., Patton, D., Sawicki, M., & Shepherd, C.W. 1999, ApJ, submitted.

Cole, S., Ellis, R. S., Broadhurst, T. J. & Colless, M. M. 1994, MNRAS, 267, 541.

Connolly, A.J., Csabai, I., Szalay, A.S., Koo, D.C., Kron, R.G., and Munn, J.A. 1995, AJ, 110, 6.

Connolly, A.J., Szalay, A.S., and Brunner, R.J. 1998, ApJ, 499, L125.

Efstathiou, G., Bernstein, G., Tyson, J. A., Katz, N. & Guhathakurta, P. 1991, ApJ, 380, L47.

Fukugita, M., Shimasaku, K., Ichikawa, T. 1995, PASP, 107, 945.

Infante, L. & Pritchet, C. J. 1995, ApJ, 439, 565.

Kasier, N. 1987, MNRAS, 227, 1.

Kauffmann, G. , Colberg, J. M., Diaferio, A. & White, S. D. M. 1999, MNRAS, 307, 529.

Koo, D.C., & Szalay, A.S. 1984, ApJ, 282, 390.

Landolt, A.U. 1992, AJ, 104, 340.

Landy, S.D. & Szalay, A.S. 1993, ApJ, 412, 64.

Lasker, B. 1996, Private Communication.

Le Fèvre, O., Hudon, D., Lilly, S.J., Crampton. D., Hammer, F. 1996, ApJ, 461, 534.

Lilly, S.J., Hammer, F., Crampton, D., & Le Fevre, O. 1995, ApJ, 455, 75.

Limber, D.N. 1954, ApJ, 119, 655.

Mould, J.R. 1993, In B.T. Soifer, editor, *Sky Surveys: Protostars to Protogalaxies*, number 43 in ASP Conference Series.

Oke, J.B., & Gunn, J.E. 1983, ApJ, 266, 713.

Peebles, P.J.E. 1980, *The Large-Scale Structure of the Universe*, Princeton University Press.

Phillipps, S. 1985, MNRAS, 212, 657

Press, W.H., Teukolsky, S.A., Vetterling, W.T., & Flannery, B.P. 1992, *Numerical Recipes in C*, Cambridge University Press, Second Edition.

Roche, N., Shanks, T., Metcalfe, N. & Fong, R. 1993, MNRAS, 263, 360.

Small, T. A., Ma, C. -P. , Sargent, W. L. W. & Hamilton, D. 1999, ApJ, 524, 31.

Steidel, C.C., Giavalisco, M., Pettini, M., Dickinson, M., & Adelberger, K.L. 1996, ApJ, 462, L17.

Szalay, A.S., Connolly, A.J., & Szokoly, G.P. 1998, AJ, 117, 68..

Weinberg, S. 1972, *Gravitation and Cosmology: Principles and Applications of the General Theory of Relativity*, John Wiley & Sons.

This preprint was prepared with the AAS LaTeX macros v5.0.

Fig. 1.— The dispersion in the empirical photometric redshift relation used in the analysis ($\sigma = 0.061$). The short solid and dashed lines are used to compare the transformation between spectroscopic redshift intervals and photometric redshift intervals.

Fig. 2.— The absolute magnitude distribution of the photometric galaxy sample in the U (top) and B (bottom) bands. The determination of the distributions used the ensemble approach (see text for more details).

Fig. 3.— The B band angular correlation function for all spectral types. The solid line is a fit to the data of a line with fixed slope $\delta = -0.8$ using the method of minimization of the absolute deviations Press *et al.* (1992).

Fig. 4.— The variation in the amplitude of the B band angular correlation function for the data presented in this paper, as well as other similar published results. The dashed line is a least squares fit to our data points, and is included merely as a visual aid. This demonstrates the excellent agreement between both our data and technique with previous results.

Fig. 5.— The evolution in the amplitude of the angular correlation function with redshift. The two lines are predictions for $\Omega_0 = 0.1$ (dotted line) and $\Omega_0 = 1.0$ (dashed line) using Limber's equation (Peebles 1980). The top panel assumes the evolution parameter derived from linear theory ($\epsilon = 0.8$), the middle panel assumes fixed clustering in proper coordinates ($\epsilon = 0.0$), and the bottom panel assumes fixed clustering in co-moving coordinates ($\epsilon = -1.2$).

Fig. 6.— The evolution in the spatial correlation scale length (r_0) with redshift, assuming $\Omega_0 = 0.1$ The data presented in this paper are indicated by open squares (□). The different panels correspond to the three different canonical values for the parameterization of the evolution in the spatial correlation function: upper panel, predictions of linear theory ($\epsilon = 0.8$), middle panel, clustering fixed in proper coordinates ($\epsilon = 0.0$), bottom panel, clustering fixed in co-moving coordinates ($\epsilon = -1.2$). Overplotted are spectroscopic survey measurements with error bars (transformed to our Cosmology using the prescription of Le Fèvre *et al.* 1996) of the correlation scale length: ($\times$) Small *et al.* 1999, ($\triangle$) Carlberg *et al.* 1999, and (■) Le Fèvre *et al.* 1996. Although not shown (in order to improve the clarity of the figure), each of our data points has an uncertainty in the horizontal direction of ± 0.1.

Fig. 7.— The evolution in the correlation scale length with both redshift and absolute U magnitude. The three panels correspond to the three different redshift intervals utilized: $0.2 \leq z \leq 0.6$ (top panel), $0.4 \leq z \leq 0.8$ (middle panel), and $0.6 \leq z \leq 1.0$ (bottom panel). The absolute magnitude ordinal is assigned as the median of the appropriate absolute magnitude bin. As a result, the error in absolute magnitude is $\pm 1.0^m$ for the first three magnitude bins, and $\pm 2.0^m$ for the last magnitude bin. In each bin, we determine the mean value for the correlation amplitude, which declines with decreasing redshift.

Fig. 8.— The evolution in the correlation scale length with both redshift and absolute B magnitude. The three panels correspond to the three different redshift intervals utilized: $0.2 \leq z \leq 0.6$ (top panel), $0.4 \leq z \leq 0.8$ (middle panel), and $0.6 \leq z \leq 1.0$ (bottom panel). The absolute magnitude ordinal is assigned as the median of the appropriate absolute magnitude bin. As a result, the error in absolute magnitude is $\pm 1.0^m$ for the first three magnitude bins, and $\pm 2.0^m$ for the last magnitude bin. In each bin, we determine the mean value for the correlation amplitude, which declines with decreasing redshift.

Table 1. The upper magnitude limit and corresponding number of objects used in the estimation of the angular correlation function for each band.

Band	M_1	M_2	M_3	M_4
U	24.44 (1266)	24.94 (2257)	25.44 (3802)	25.94 (5668)
B	23.76 (812)	24.26 (1524)	24.76 (2685)	25.26 (4365)
R	22.95 (1003)	23.45 (1647)	23.95 (2673)	24.45 (4035)
I	22.47 (1002)	22.97 (1579)	23.47 (2429)	23.97 (3602)

Table 2. The amplitude A_w of the angular correlation function at $\theta = 1.0''$ assuming a relation $w(\theta) = A_w \theta^{-0.8}$ for the different magnitude intervals.

Band	M_1	M_2	M_3	M_4
U	0.81	0.70	0.69	0.60
B	1.23	0.87	0.84	0.73
R	1.80	1.26	1.03	0.94
I	1.87	1.42	1.08	0.94

Table 3. The measured correlation scale length and corresponding error at different redshifts for $\Omega_0 = 0.1$ and different values of the evolutionary parameters (ϵ).

	$r_0(z)$		
z	$\epsilon = 0.8$	$\epsilon = 0.0$	$\epsilon = -1.2$
0.4	4.03 (+1.01/-1.41)	3.47 (+0.87/-1.21)	2.76 (+0.69/-0.96)
0.6	3.71 (+0.67/-0.78)	2.99 (+0.54/-0.63)	2.16 (+0.39/-0.46)
0.8	4.23 (+0.85/-1.32)	3.26 (+0.65/-1.02)	2.20 (+0.44/-0.69)
1.0	3.83 (+1.22/-1.31)	2.86 (+0.91/-0.98)	1.85 (+0.59/-0.63)

Table 4. The correlation scale length and associated errors extrapolated to $z = 0.0$ for different values of Cosmological and Evolutionary parameters.

Ω_0	$r_0(z=0)$ $\epsilon = 0.8$	$\epsilon = 0.0$	$\epsilon = -1.2$
0.1	3.98 (+0.65/-1.12)	3.69 (+0.65/-1.07)	3.19 (+0.61/-0.95)
0.3	3.94 (+0.66/-1.11)	3.63 (+0.66/-1.05)	3.12 (+0.68/-0.93)
1.0	3.76 (+0.66/-1.09)	3.43 (+0.64/-1.01)	2.91 (+0.58/-0.88)

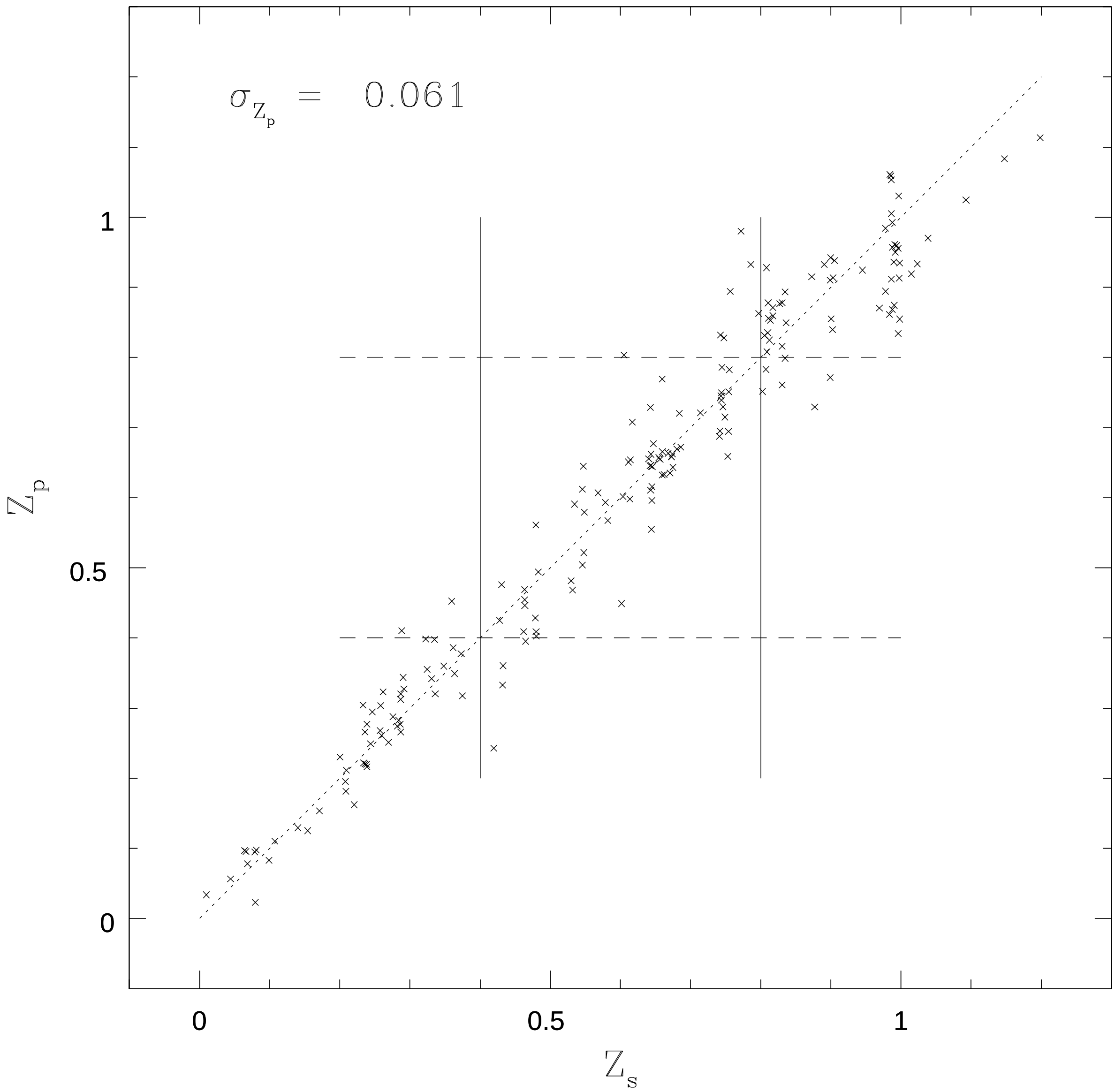
σ_{Z_p} = 0.061
Z_p
1
0.5
0
0
0.5
1
Z_s

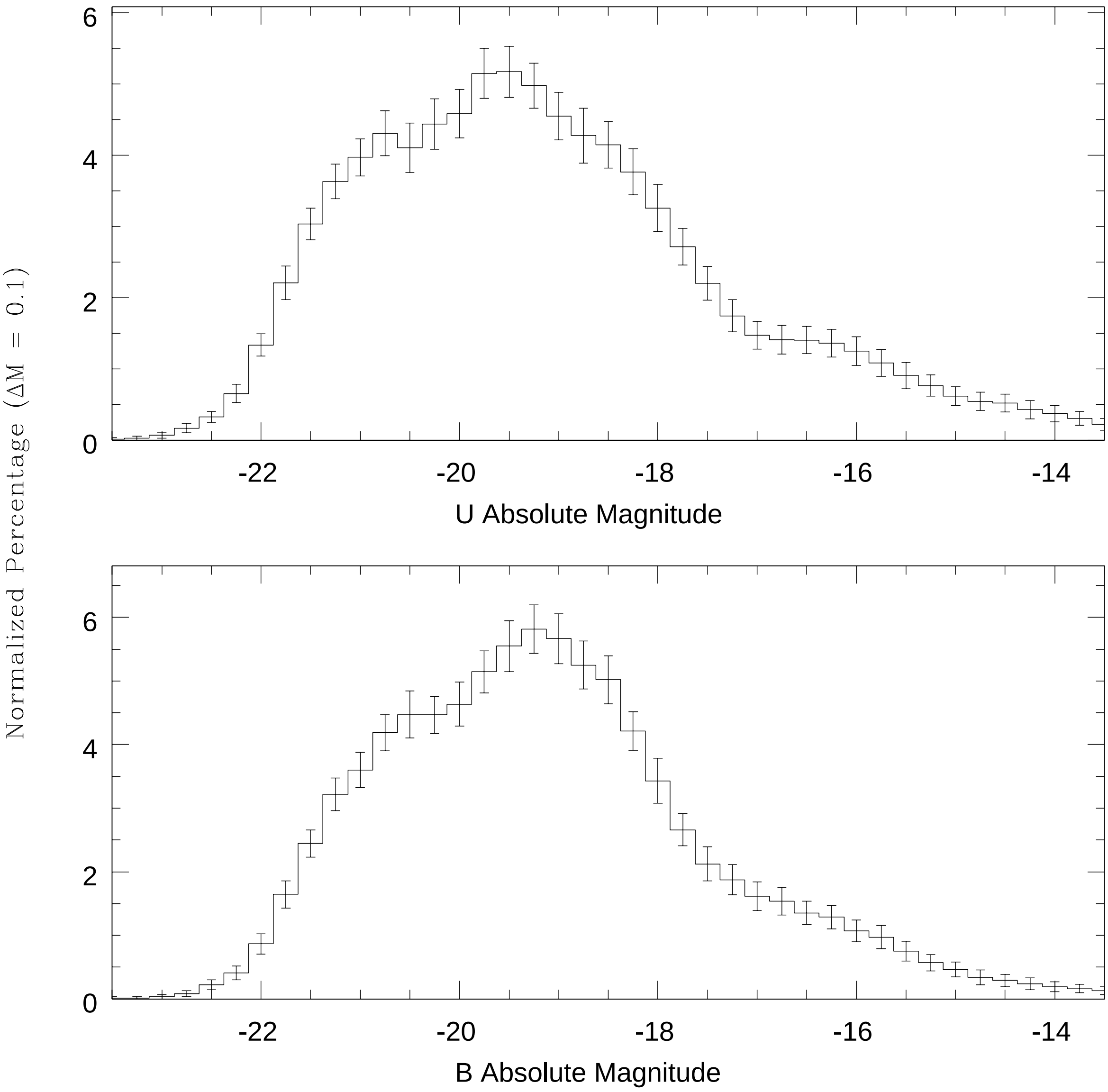
Normalized Percentage (ΔM = 0.1)
6
4
2
0
-22
-20
-18
-16
-14
U Absolute Magnitude
6
4
2
0
-22
-20
-18
-16
-14
B Absolute Magnitude

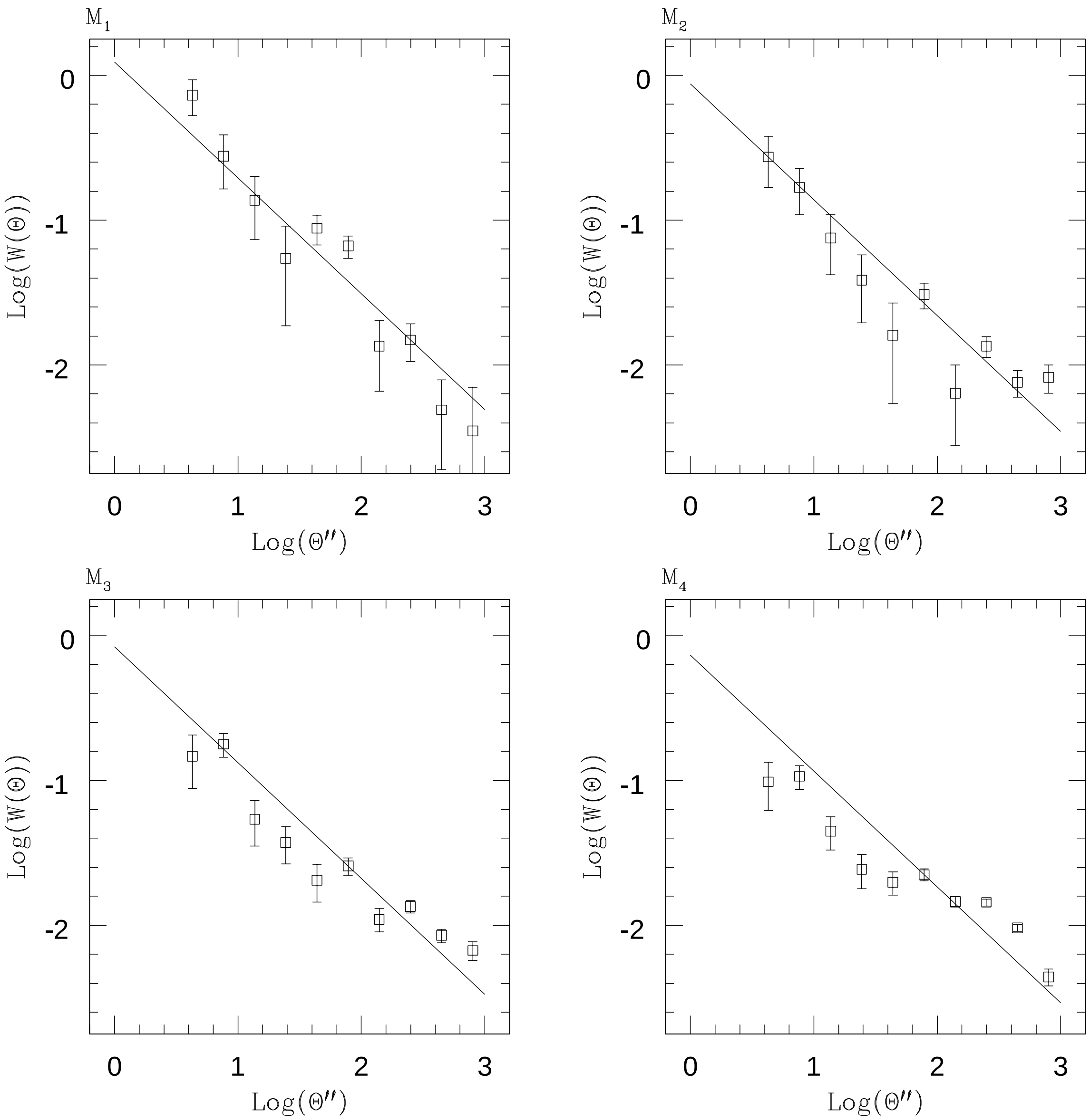
M1
M2
M3
M4
Log(W(Θ))
Log(Θ″)
0
-1
-2
0
1
2
3

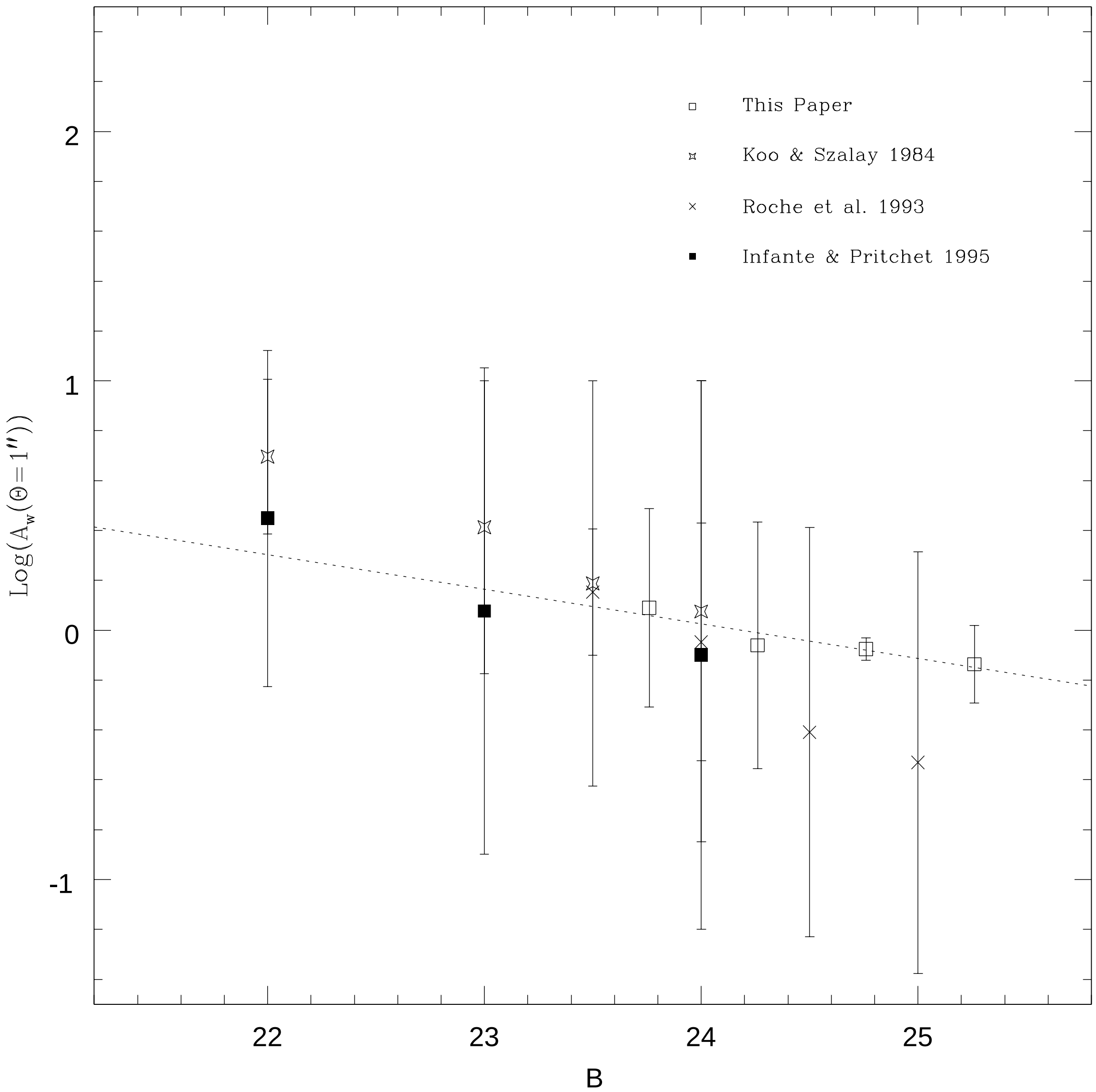
This Paper
Koo & Szalay 1984
Roche et al. 1993
Infante & Pritchet 1995
Log(A_w(Θ=1″))
B
2
1
0
-1
22
23
24
25

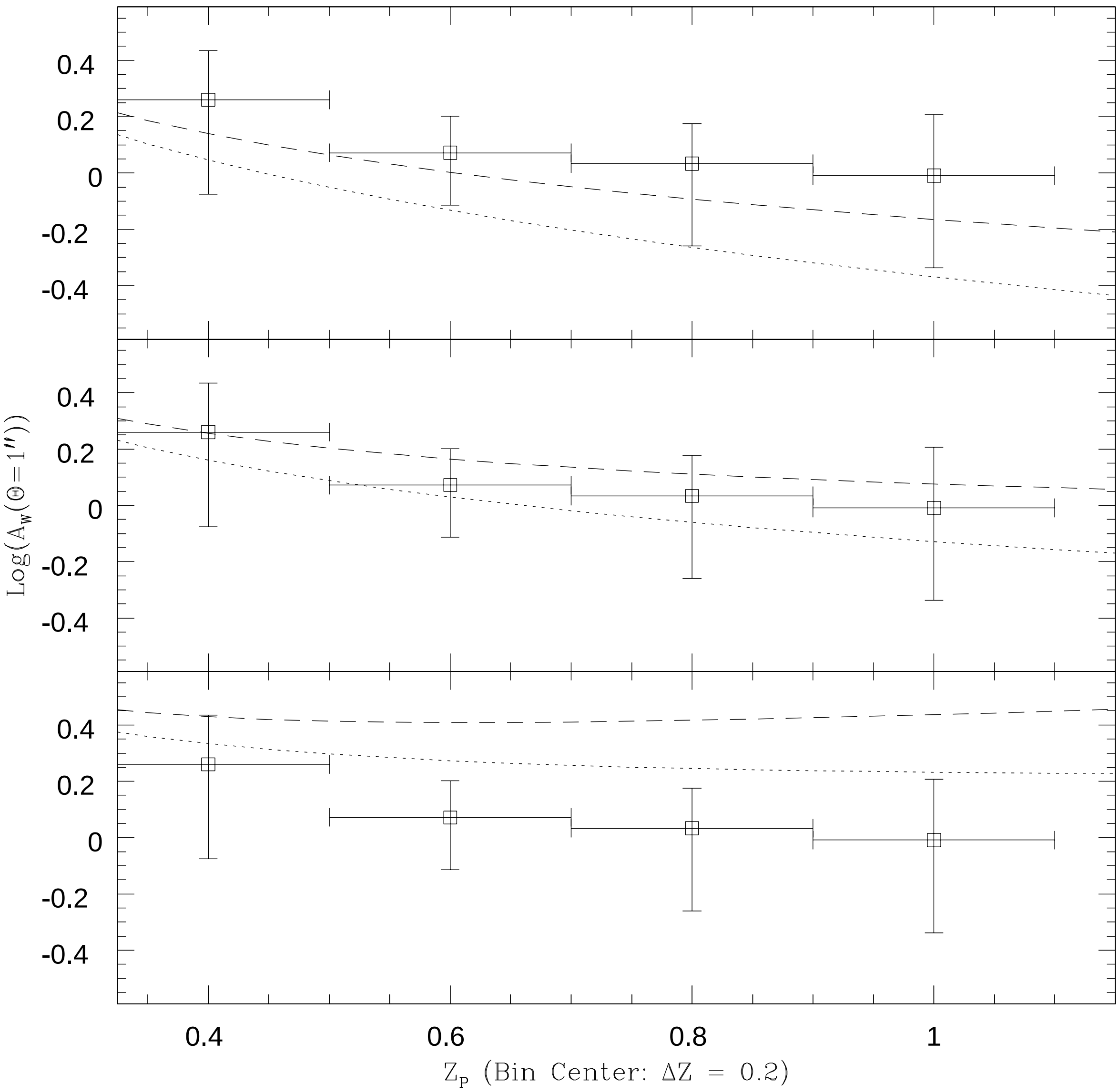
0.4
0.2
0
-0.2
-0.4
Log(A_W(Θ=1″))
0.4
0.6
0.8
1
Z_p (Bin Center: ΔZ = 0.2)

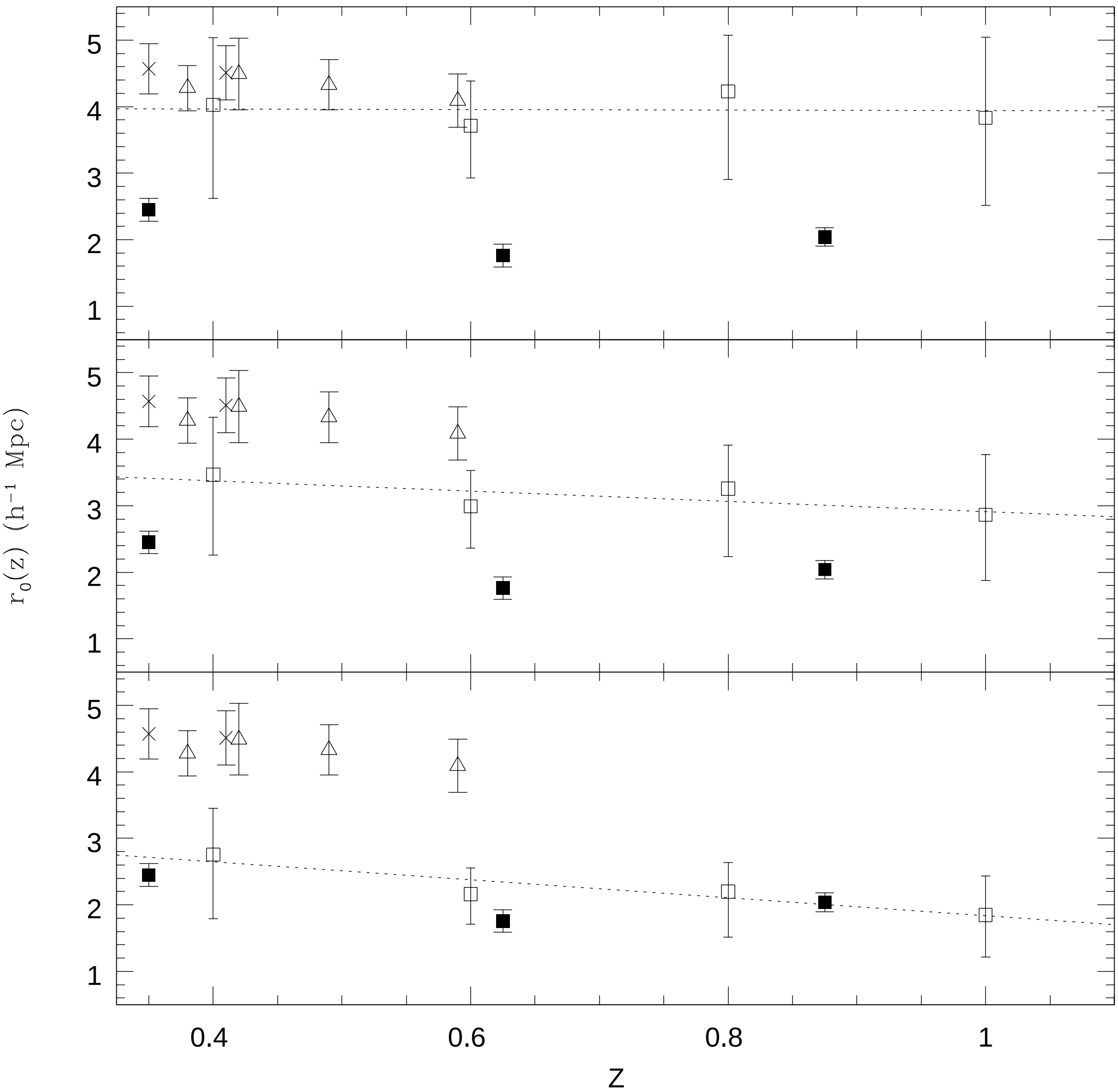
$r_0(z)$ (h^{-1} Mpc)
1
2
3
4
5
0.4
0.6
0.8
1
Z

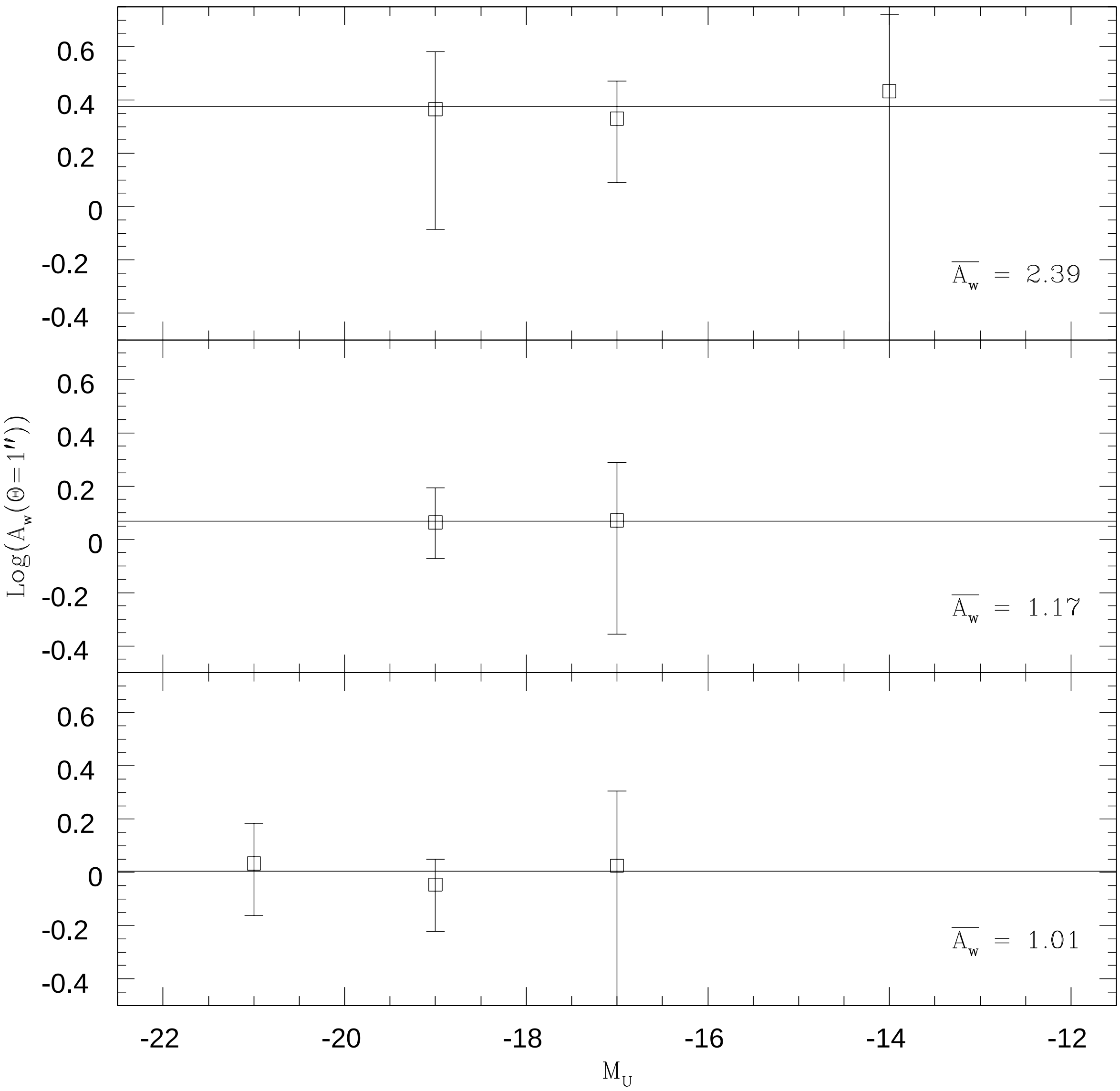

0.6
0.4
0.2
0
-0.2
-0.4
$\overline{A_w}$ = 2.39
$\overline{A_w}$ = 1.17
$\overline{A_w}$ = 1.01
Log(A$_w$(Θ=1″))
-22
-20
-18
-16
-14
-12
M$_U$

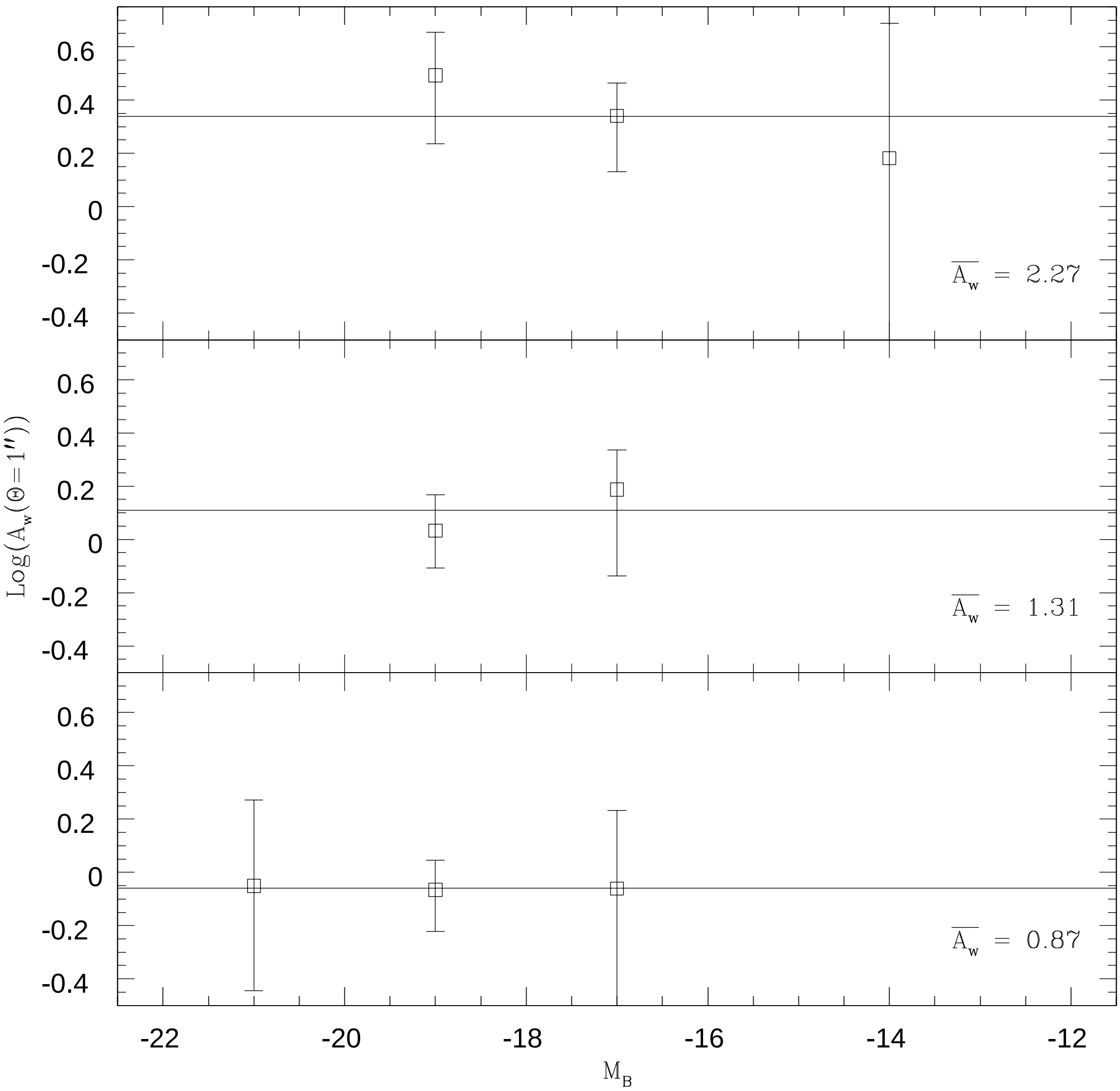
0.6
0.4
0.2
0
-0.2
-0.4
$\overline{A_w}$ = 2.27
$\overline{A_w}$ = 1.31
$\overline{A_w}$ = 0.87
Log(A_w(Θ=1″))
-22
-20
-18
-16
-14
-12
M_B